Available online at www.sciencedirect.com

ScienceDirect

Mendeleev Commun., 2023, **33**, 673–675

Mendeleev Communications

Preparation of supported single-phase Pd_xIn_y intermetallic nanoparticles

Alexander V. Rassolov,* Pavel V. Markov, Galina N. Baeva, Dmitriy A. Bokarev, Artem R. Kolyadenkov, Anastasia E. Vaulina and Alexander Yu. Stakheev

N. D. Zelinsky Institute of Organic Chemistry, Russian Academy of Sciences, 119991 Moscow, Russian Federation. Fax: +7 499 135 5328; e-mail: rav@ioc.ac.ru

DOI: 10.1016/j.mencom.2023.09.026

The use of conventional co-impregnation methods makes it possible to synthesize supported Pd_xIn_y nanoparticles with defined stoichiometry, which is determined by the ratio of components during the preparation stage. The phase composition and surface structure of the intermetallic nanoparticles is determined using FTIR-CO, TEM, and XRD analysis.

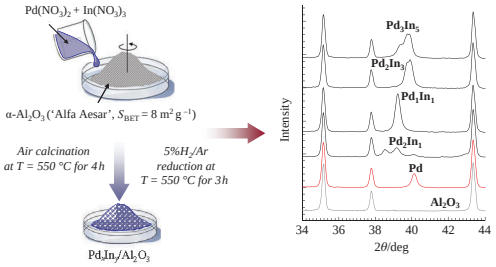

Keywords: Pd–In, DRIFT spectroscopy of adsorbed CO, intermetallics, XRD, palladium-based alloy, nanoparticles, isolated Pd sites.

Currently, catalysts based on intermetallic nanoparticles are promising systems for the development of highly stable and selective catalytic materials with unique properties.[1–4] Unlike substitutional alloys, intermetallics are single-phase stoichiometric compounds consisting of two or more metals with different electonegativity, and their crystal structure differs from the structures of individual components. Due to partially covalent or ionic bonds in the intermetallics, a higher structural stability is often observed, especially, against segregation.[4–8] In addition, intermetallic structures possess high thermodynamic stability over a wide temperature range.[7]

A unique advantage of intermetallic catalysts is the ability to tune their crystal structure and electronic characteristics by varying the ratio between components at the stage of preparation. This feature and the high stability of intermetallic structures makes it possible to adjust the catalytic characteristics depending on a specific process.

The development of methods for the preparation of intermetallic nanoparticles supported on an inert carrier is of interest in both industrial applications and laboratory practice. This task is not trivial because it is especially important to obtain supported nanoparticles of identical phase composition and to avoid the formation of nanoparticles consisting of various intermetallic phases.

In this work, we focused on the preparation of single-phase Pd_xIn_y nanoparticles supported on α-Al_2O_3. These systems are promising model catalysts for studying relationships between the structure of intermetallic nanoparticles and their catalytic performance in different reactions.

The Pd_xIn_y intermetallics were chosen because they can form a series of intermetallic structures with different crystallographic and electronic characteristics depending on the Pd/In atomic ratio. They are of interest due to the remarkable catalytic performance in various processes, such as formic acid oxidation,[9] ethanol oxidation,[10] ethane dehydrogenation,[11] selective gas-phase and liquid-phase hydrogenation,[12,13] methanol steam reforming,[8,14] and methanol synthesis. A comparative study of the catalytic characteristics of the Pd_xIn_y intermetallics in the liquid-phase hydrogenation of CO_2 into methanol revealed superior activity of a Pd_1In_1 intermetallic compared to that of a reference In_2O_3 catalyst and monometallic Pd.[15] In the gas-phase hydrogenation of carbon dioxide to methanol, the best performance was observed with a Pd_1In_2/SiO_2 catalyst.[16]

The supported Pd_xIn_y nanoparticles were prepared using conventional co-impregnation methods (for details, see Online Supplementary Materials, Table S1).

Note that the crystal structure of supported intermetallic nanoparticles is difficult to characterize because it is difficult to separate the signals of an intermetallic phase from the background signals of an oxide support. In order to avoid this problem, we used α-Al_2O_3 as a carrier for the preparation of Pd_xIn_y/Al_2O_3 intermetallic samples. The well crystalline structure of α-Al_2O_3 makes it possible to reliably examine Pd_xIn_y nanoparticles by XRD analysis because the support reflexes are narrow, and they do not overlap with the characteristic signals of Pd, In, or Pd_xIn_y intermetallic compounds. In addition, the high chemical inertness of this carrier minimizes the metal–support interactions.

Figure 1 depicts XRD patterns of the α-Al_2O_3 support, monometallic Pd, and samples with Pd : In molar ratios from 3 : 5 to 1 : 1 in the range 2θ = 34–54°. The diffraction peaks of α-Al_2O_3 were detected at 2θ of 35.2, 37.8, 43.4, and 52.6° (ICSD 10425). The small width of these signals indicates the good crystallinity of the support.[17] The XRD pattern of a monometallic Pd sample exhibited reflexes at 40.1 and 46.6° characteristic of the (111) and (200) facets of the face-centered cubic (fcc) lattice of monometallic Pd, respectively (ICSD 52251).

The diffraction pattern of a sample loaded with 3.0 wt% Pd and 1.6 wt% In was characterized by peaks at 38.5, 39.1, 40.1, and 46.3°, indicating the formation of orthorhombic α-Pd_2In (PDF 04-014-9340). The particle size calculated on the basis of

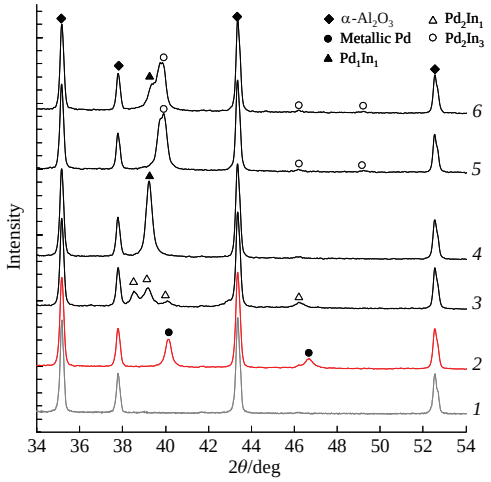

Figure 1 XRD patterns for the samples of (*1*) α-Al_2O_3, (*2*) Pd/α-Al_2O_3 (reference), (*3*) Pd_2In_1/α-Al_2O_3, (*4*) Pd_1In_1/α-Al_2O_3, (*5*) Pd_2In_3/α-Al_2O_3, and (*6*) Pd_3In_5/α-Al_2O_3.

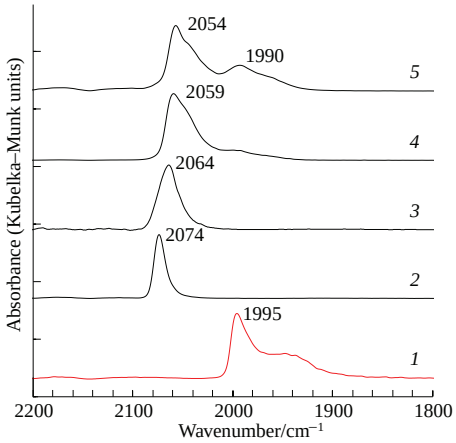

Figure 2 DRIFT spectra of adsorbed CO on the samples of (*1*) Pd/α-Al_2O_3 (reference), (*2*) Pd_1In_1/α-Al_2O_3, (*3*) Pd_2In_1/α-Al_2O_3, (*4*) Pd_2In_3/α-Al_2O_3, and (*5*) Pd_3In_5/α-Al_2O_3.

XRD peak broadening by the Scherrer equation was consistent with TEM data (10.3 and 8.8 nm, respectively).

The reflex of a sample with 3.0 wt% Pd and 3.2 wt% In at 2θ of 39.2° demonstrated the presence of an intermetallic PdIn phase with a cubic CsCl-type structure (PDF 04-004-1991). The measured size of nanoparticles (9.7 nm) was also consistent with TEM data. The Pd_1In_1 compound is mentioned as the most common of all possible Pd_xIn_y structures,[18,19] though the Pd_1In_1 structure can exist in a wide range of Pd concentrations (from 45–50 to ~55–57 at% Pd).[20] It should be assigned that the formation of an intermetallic compound with an equimolar Pd : In ratio is more preferable due to the similarity of its crystal structure to the fcc structure of metallic Pd. Therefore, no significant rearrangements of Pd atoms are required.[11]

In the diffraction pattern of a sample containing 3.0 wt% Pd and 4.8 wt% In, reflexes at 2θ of about 39.9, 46.2, and 49.3° were observed. These signals indicated the formation of a large well-crystallized Pd_2In_3 intermetallic structure (PDF 04-004-8804). A small shoulder in a range of 2θ from 38.7 to 39.1° corresponds to the reflection of the Pd_1In_1 phase. The average size of nanoparticles was about 11.0 nm.

The diffraction pattern of the Pd_3In_5 sample shows signals from two phases of intermetallic compounds, the composition of which does not correspond to that specified at the preparation stage. The signals at 2θ = 39.9, 46.2, and 49.3° correspond to a Pd_2In_3 intermetallic phase, while a pronounced shoulder in the range 2θ = 39.0–39.5° [Figure 1, curve (*6*)], as in case of the previous sample, indicates the formation of an intermetallic phase with a Pd : In ratio of 1 : 1.

Note that the test Pd_xIn_y intermetallic samples showed no peaks that are characteristic of monometallic Pd^0. The In^0 metal particles were also not detected, as indicated by the absence of characteristic XRD reflexes at 36.2 and 39.1° related to the (002) and (110) planes of In crystals, respectively.

The size and shape of nanoparticles were studied by TEM. Typical micrographs and histograms of the size distribution of nanoparticles are presented in Figure S1 (see Online Supplementary Materials). The formation of large irregularly shaped nanoparticles from 10 to 50 nm was observed in a monometallic Pd [Figure S1(*a*)] sample. The average size of nanoparticles was 31 nm. Formation of relatively massive (~50–60 nm) and smaller spherical nanoparticles (4–10 nm) was typical of intermetallic Pd_xIn_y samples [Figure S1(*b*)–(*e*)]. The average size of nanoparticles in the Pd_xIn_y catalysts ranged from 8 to 11 nm, and it was almost independent of the Pd : In ratio. All Pd_xIn_y samples were characterized by a monomodal Gaussian size distribution.

The CO-DRIFTS technique was used for studying the surface structure. Figure 2 shows typical IR spectra of CO adsorbed on the surface of monometallic Pd and Pd_xIn_y samples with different component ratios.

The spectrum of CO adsorbed on the reference monometallic Pd exhibits only a broad band at 2010–1880 cm^{-1} corresponding to the adsorption on two neighboring atoms (bridged adsorbed CO in a range from 2010 to 1900 cm^{-1}) and threefold bridged CO (~1900–1880 cm^{-1}).[21] The characteristic band of on top Pd atom adsorption (linear adsorbed in a range from 2200 to 2000 cm^{-1}) is almost absent.[22]

The spectra of intermetallic samples are significantly different. For Pd_2In_1, the only intense asymmetric absorption band at 2074 cm^{-1} was detected. It was attributed to linear adsorbed CO on Pd atoms of PdIn nanoparticles. The absence of other bands not only indicates an increase in the Pd–Pd interatomic distance but also shows the formation of an intermetallic Pd_xIn_y structure with isolated Pd_1 atoms.[23,24]

Similar spectra of linear adsorbed CO were obtained for Pd–Ga intermetallic catalysts.[25] The Pd–Ga compositions displayed an increased stability and an extremely high selectivity in the gas-phase hydrogenation of acetylene. The results were interpreted using the concept of site-isolated catalysts, which is closely related to the concept of single-atom catalysts. Isolation of individual Pd atoms by adjacent Ga atoms in the intermetallics was confirmed with both theoretical calculations and physicochemical analysis (*in situ* XPS and FTIR-CO).

An increase in the concentration of In leads to a gradual shift of the position of a linear CO band toward lower wavenumbers. The maxima of the Pd_2In_1 and for Pd_1In_1 samples are at 2074 and 2064 cm^{-1}, respectively. This shift can be caused by increasing electron density at the Pd atoms in the intermetallic compound. This, in turn, promotes an increase in electron density donation from Pd atoms to the π-antibonding orbital of the CO molecule, followed by a change of the electronic state of an intermetallic Pd component.[26] Note that the shift observed for the maximum of a linear adsorption form was accompanied by an increase in the gradual asymmetry and the absorption band width.

This effect may be due to the adsorption of CO on different crystallographic phases. Thus, CO adsorption occurred on the (110) and (111) faces of the intermetallic compound Pd_1In_1.[27] The DFT results displayed that the multipoint adsorption of CO on the surface of Pd_xIn_y nanoparticles is unfavorable. The energy of CO adsorption in the bridge position on PdIn (110) was insignificant (–0.09 eV) due to a large distance between neighboring Pd atoms.

Adsorption of bridging CO on the PdIn(111) face is also impossible because the Pd atoms adjacent to the surface Pd atom are located significantly below the surface plane. Since the nearest Pd surface atom is at a distance of 4.73 Å, this makes bridging CO adsorption impossible.

However, the Pd_2In_3 sample exhibited a linear adsorbed CO band shift to lower wavenumbers relatively to that of the Pd_1In_1 sample (2064 and 2059 cm^{-1}, respectively). In addition, an increase in the characteristic bridging and threefold absorption bands was observed, as in the monometallic Pd sample.

Similar results were obtained for the Pd_3In_5 sample, which also displayed a shift of the absorption band of linear CO (at 2054 cm^{-1}) and a broad band due to bridging adsorption at 1990 cm^{-1}.

A reason for an increase in the intensity of the bridging absorption band may be the formation of defects in the crystal structure of higher intermetallic compounds. These defects can be due to the formation of a more thermodynamically stable Pd_1In_1 intermetallic phase in addition to the main phase, which was confirmed by the XRD data.[28–30] In this case, defects at the grain boundary[31] can contribute to the formation of multicoordinated CO adsorption active sites.

Thus, the results clearly demonstrated that supported single-phase Pd_xIn_y nanoparticles with average sizes from 9 to 11 nm and with a strictly defined stoichiometry (Pd_2In_1, Pd_1In_1) can be synthesized using a co-impregnation method. For model samples with high Pd : In ratios (2 : 3 and 3 : 5), it is more difficult to obtain single-phase intermetallic nanoparticles. In these samples, we observed the formation of two intermetallic phases of Pd_2In_3 and Pd_1In_1. For Pd_2In_3, the fraction of Pd_1In_1 is minor, while the contribution of Pd_1In_1 for Pd_3In_5 becomes significant.

This work was supported by the Russian Science Foundation (grant no. 23-23-00510). The authors are grateful to the Department of Structural Studies at N. D. Zelinsky Institute of Organic Chemistry of the Russian Academy of Sciences for the TEM characterization of samples.

Online Supplementary Materials

Supplementary data associated with this article can be found in the online version at doi: 10.1016/j.mencom.2023.09.026.

References

1 V. S. Marakatti and S. C. Peter, *Prog. Solid State Chem*., 2018, **52**, 1.
2 A. Dasgupta and R. M. Rioux, *Catal. Today*, 2019, **330**, 2.
3 M. Krajčí and J. Hafner, *ChemCatChem*, 2016, **8**, 34.
4 M. Armbrüster, in *Encyclopedia of Catalysis*, ed. I. T. Horváth, Wiley, Weinheim, 2011, https://doi.org/10.1002/0471227617.eoc220.
5 P. Wu, J. Zaffran and B. Yang, *J. Phys. Chem. C*, 2019, **123**, 13615.
6 I. Sharafutdinov, C. F. Elkjær, H. W. Pereira de Carvalho, D. Gardini, G. L. Chiarello, C. D. Damsgaard, J. B. Wagner, J.-D. Grunwaldt, S. Dahl and I. Chorkendorff, *J. Catal*., 2014, **320**, 77.
7 S. Furukawa and T. Komatsu, *ACS Catal*., 2017, **7**, 735.
8 K. Föttinger, *Catalysis*, 2013, **25**, 77.
9 R. Zhang, M. Peng, L. Ling and B. Wang, *Chem. Eng. Sci.*, 2019, **199**, 64.
10 Y.-J. Chen, Y.-R. Chen, C.-H. Chiang, K.-L. Tung, T.-K. Yeh and H.-Y. Tuan, *Nanoscale*, 2019, **11**, 3336.
11 Q. Feng, S. Zhao, Y. Wang, J. Dong, W. Chen, D. He, D. Wang, J. Yang, Y. Zhu, H. Zhu, L. Gu, Z. Li, Y. Liu, R. Yu, J. Li and Y. Li, *J. Am. Chem. Soc.*, 2017, **139**, 7294.
12 Y. Cao, Z. Sui, Y. Zhu, X. Zhou and D. Chen, *ACS Catal*., 2017, **7**, 7835.
13 I. S. Mashkovsky, P. V. Markov, G. O. Bragina, G. N. Baeva, A. V. Rassolov, I. A. Yakushev, M. N. Vargaftik and A. Yu. Stakheev, *Nanomaterials*, 2018, **8**, 769.
14 F. Sha, Z. Han, S. Tang, J. Wang and C. Li, *ChemSusChem*, 2020, **13**, 6160.
15 A. García-Trenco, A. Regoutz, E. R. White, D. J. Payne, M. S. P. Shaffer and C. K. Williams, *Appl. Catal., B*, 2018, **220**, 9.
16 J. L. Snider, V. Streibel, M. A. Hubert, T. S. Choksi, E. Valle, D. C. Upham, J. Schumann, M. S. Duyar, A. Gallo, F. Abild-Pedersen and T. F. Jaramillo, *ACS Catal*., 2019, **9**, 3399.
17 Z. Li, K. Wu, J. Cao and Y. Wang, *IOP Conf. Ser.: Mater. Sci. Eng.*, 2017, **207**, 012004.
18 H. Lorenz, S. Turner, O. I. Lebedev, G. van Tendeloo, B. Klötzer, C. Rameshan, K. Pfaller and S. Penner, *Appl. Catal., A*, 2010, **374**, 180.
19 M. Neumann, D. Teschner, A. Knop-Gericke, W. Reschetilowski and M. Armbrüster, *J. Catal*., 2016, **340**, 49.
20 H. Okamoto, *J. Phase Equilib*., 2003, **24**, 481.
21 G. Agostini, R. Pellegrini, G. Leofanti, L. Bertinetti, S. Bertarione, E. Groppo, A. Zecchina and C. Lamberti, *J. Phys. Chem. C*, 2009, **113**, 10485.
22 N. S. Smirnova, G. N. Baeva, P. V. Markov, I. S. Mashkovsky, A. V. Bukhtiyarov, Ya. V. Zubavichus and A. Yu. Stakheev, *Mendeleev Commun.*, 2022, **32**, 807.
23 D. B. Burueva, K. V. Kovtunov, A. V. Bukhtiyarov, D. A. Barskiy, I. P. Prosvirin, I. S. Mashkovsky, G. N. Baeva, V. I. Bukhtiyarov, A. Yu. Stakheev and I. V. Koptyug, *Chem. – Eur. J*., 2018, **24**, 2547.
24 S. Furukawa, M. Endo and T. Komatsu, *ACS Catal*., 2014, **4**, 3533.
25 K. Kovnir, M. Armbrüster, D. Teschner, T. V. Venkov, F. C. Jentoft, A. Knop-Gericke, Y. Grin and R. Schlögl, *Sci. Technol. Adv. Mater.*, 2007, **8**, 420.
26 K. Föttinger, J. A. van Bokhoven, M. Nachtegaal and G. Rupprechter, *J. Phys. Chem. Lett.*, 2011, **2**, 428.
27 N. S. Smirnova, I. S. Mashkovsky, P. V. Markov, A. V. Bukhtiyarov, G. N. Baeva, H. Falsig and A. Yu. Stakheev, *Catalysts*, 2021, **11**, 1376.
28 W. E. Liu and S. E. Mohney, *Mater. Sci. Eng.: B*, 2003, **103**, 189.
29 J. M. Bird, A. W. Bryant and J. N. Pratt, *J. Chem. Thermodyn.*, 1975, **7**, 577.
30 Z. Wu, E. C. Wegener, H.-T. Tseng, J. R. Gallagher, J. W. Harris, R. E. Diaz, Y. Ren, F. H. Ribeiro and J. T. Miller, *Catal. Sci. Technol.*, 2016, **6**, 6965.
31 A. B. Kuriganova, M. S. Lipkin and N. V. Smirnova, *Mendeleev Commun.*, 2021, **31**, 224.

Received: 12th May 2023; Com. 23/7169